IMPACT OF NANOFLUIDS AND MAGNETIC FIELD ON THE PERISTALTIC TRANSPORT OF A COUPLE STRESS FLUID IN AN ASYMMETRIC CHANNEL WITH DIFFERENT WAVE FORMS

by

***Safia AKRAM*[a*], *Farkhanda AFZAL*[a], *and Qamar AFZAL*[b]**

[a] MCS, National University of Sciences and Technology, Islamabad, Pakistan
[b] Department of Mathematics and Statistics, University of Lahore, Lahore, Pakistan

Original scientific paper
https://doi.org/10.2298/TSCI190720389A

The present article deals with the effects of nanoparticles and magnetic field on the peristaltic flow of a couple stress fluid in an asymmetric channel with different wave forms. Mathematical modelling for 2-D and two directional flows of a couple stress fluid along with nanofluid are first given and then simplified under the assumptions of long wavelength and low Reynolds number approximation. After invoking these approximations we get coupled non-linear differential equations. The exact solutions of temperature distribution, the nanoparticle concentration, velocity, stream function and pressure gradient are calculated. Finally graphical results of various physical parameters of interest are discussed to examine the behavior of flow quantities.

Key words: *nanofluid particles, peristaltic flow, asymmetric channel, couple stress fluid, magnetic field, different wave forms*

Introduction

Nanofluids are those liquids which contain a small quantity of nanoparticles in suspension which have a size of roughly 1000^{th} of the width of a human hair. These liquids possess high rate of heat transfer than any other liquid made by other theories. This makes them very attractive as heat transfer fluids in many applications. These are used in electronics, nuclear reactors, transportation, electronics, biomedicine and food. These are also applicable as coolants in welding equipment and automobiles industries. Due to the applications in sciences and industry nanofluids have achieved considerable importance among the researchers. The first investigation on nanofluids was done by Choi [1]. Later on based on the theory develop by Choi [1], many research discussed the phenomena of nanofluids using different flow geometries [2-5]. However, only limited attentions have been given to the peristaltic flows of nanofluids [6-10].

Peristalsis is a mechanism of fluid transport induces by a progressive wave of area contraction or expansion along the flexible walls of a channel. These flows are used for transport of blood in vessels. Pumping is the most common industrial use of peristaltic flow. In the urinary system drives urine from the kidneys to the bladder through the ureters this peristalsis is due to involuntary muscular contractions of the ureteral wall. Fluid trapping and material reflux are two interesting phenomena associated with peristaltic flows. The mechanism of peristaltic flow has attracted the attention of many researchers since the first exploration done by Latham

* Corresponding author, e-mail: drsafiaakram@gmail.com; safia_akram@yahoomail.com

[11], many researchers have discussed the peristaltic flows of Newtonian and non-Newtonian fluids with different flow geometries [12-16]. Most of these investigations are restricted to the peristaltic flow only in a symmetric channel, tube and cylinder.

Recently, physiologists observed that the intra-uterine fluid flow due to myometrial contractions is peristaltic type motion and the myometrial contractions may occur in both symmetric and asymmetric directions. The importance of peristaltic flows in asymmetric channel has been highlighted by Eytan and Elad [17]. Akram *et al.* [18, 22], Akram [19], Nadeem *et al.* [20], and Nadeem and Akram [21] have examined the peristaltic flows of Newtonian and non-Newtonian fluids in an asymmetric channel. Yilidirim and Sezer [23] talk about the effects of partial slip on the peristaltic flow of a MHD Newtonian fluid in an asymmetric channel. The peristaltic transport on third and fourth grade fluids has examined by Haroun [24, 25]. Some interesting studies dealing with asymmetric channel are given in Refs [26-30].

Motivated from the aforementioned study, the aim of the current paper is to inspect the impact of nanoparticles and magnetic field on the peristaltic transport of a couple stress fluid in an asymmetric channel. The governing equations of couple stress fluid, teat transfer and nanoparticle volume fraction for 2-D flow in Cartesian co-ordinate system are first modelled and then simplified under the lubrication approach. The exact solution of temperature, nanoparticle volume fraction, velocity and stream function are calculated. The physical features of the relevant parameters are considered by plotting the graphs of velocity, pressure rise, pressure gradient, temperature, concentration and stream lines along with different wave forms.

Mathematical formulation

Let us consider the peristaltic flow of an incompressible, electrically conducting couple stress fluid in a 2-D channel of width $d_1 + d_2$. The flow is generated by sinusoidal wave trains propagating with constant speed c along the channel walls. We choose rectangular co-ordinate system for the channel with X along the centerline of the channel and Y is transverse to it. The left wall of the channel is maintained at temperature, T_1, while the right wall has temperature, T_0. We seek the velocity field for the 2-D and two directional flow of the form $\mathbf{V} = [U(X, Y, t), V(X, Y, t), 0]$. Moreover, we assume that the fluid is subject to a constant transverse magnetic field, B_0. A very small magnetic Reynolds number is assumed and hence the induced magnetic field can be neglected. When the fluid moves into magnetic field two major physical effects arise. The first one is that an electric field $\mathbf{E}$ is induced in the flow. We shall assume that there is no excess charge density and therefore, $\nabla\mathbf{B} = 0$. Neglecting the induced magnetic field implies that $\nabla\mathbf{E} = 0$ and therefore, the induced electric field is negligible. The second effect is dynamically in nature, *i. e.*, a Lorentz force $(\mathbf{J}\times\mathbf{B})$, where $\mathbf{J}$ is the current density, this force acts on the fluid and modifies its motion. This results in the transfer of energy from the electromagnetic field to the fluid. In present study, the relativistic effects are neglected and the current density $\mathbf{J}$ is given by the Ohm's law as $\mathbf{J} = \sigma(\mathbf{V}\times\mathbf{B})$.

The geometry of the wall surface is defined:

$$Y = H_1(X,t) = d_1 + a_1\cos\left[\frac{2\pi}{\lambda}(X - ct)\right], \quad Y = H_2(X,t) = -d_2 - b_1\cos\left[\frac{2\pi}{\lambda}(X - ct) + \phi\right] \tag{1}$$

In fixed frame, the equations of continuity, momentum and nanofluid for couple stress fluid, in presence of applied magnetic field are defined:

$$\frac{\partial U}{\partial X} + \frac{\partial V}{\partial Y} = 0 \tag{2}$$

$$\rho_f\left(\frac{\partial U}{\partial t}+U\frac{\partial U}{\partial X}+V\frac{\partial U}{\partial Y}\right)=-\frac{\partial P}{\partial X}+\mu\left(\frac{\partial^2 U}{\partial Y^2}+\frac{\partial^2 U}{\partial X^2}\right)-\eta\left(\frac{\partial^4 U}{\partial Y^4}+\frac{\partial^4 U}{\partial X^4}+2\frac{\partial^4 U}{\partial X^2\partial Y^2}\right)-$$
$$-\sigma B_0^2 U+\rho g\alpha\left(T_1-T_0\right)+\rho g\alpha\left(C_1-C_0\right) \tag{3}$$

$$\rho_f\left(\frac{\partial V}{\partial t}+U\frac{\partial V}{\partial X}+V\frac{\partial V}{\partial Y}\right)=-\frac{\partial P}{\partial Y}+\mu\left(\frac{\partial^2 V}{\partial Y^2}+\frac{\partial^2 V}{\partial X^2}\right)-\eta\left(\frac{\partial^4 V}{\partial Y^4}+\frac{\partial^4 V}{\partial X^4}+2\frac{\partial^4 V}{\partial X^2\partial Y^2}\right) \tag{4}$$

$$\left(\frac{\partial T}{\partial t}+U\frac{\partial T}{\partial X}+V\frac{\partial T}{\partial Y}\right)=$$
$$=\alpha\left(\frac{\partial^2 T}{\partial X^2}+\frac{\partial^2 T}{\partial Y^2}\right)+\tau\left\{D_B\left(\frac{\partial C}{\partial X}\frac{\partial T}{\partial X}+\frac{\partial C}{\partial Y}\frac{\partial T}{\partial Y}\right)\left(\frac{D_T}{T_0}\right)\left[\left(\frac{\partial T}{\partial X}\right)^2+\left(\frac{\partial T}{\partial Y}\right)^2\right]\right\} \tag{5}$$

$$\left(\frac{\partial C}{\partial t}+U\frac{\partial C}{\partial X}+V\frac{\partial C}{\partial Y}\right)=D_B\left(\frac{\partial^2 C}{\partial X^2}+\frac{\partial^2 C}{\partial Y^2}\right)+\left(\frac{D_T}{T_0}\right)\left(\frac{\partial^2 T}{\partial X^2}+\frac{\partial^2 T}{\partial Y^2}\right) \tag{6}$$

where U, V are the velocities in X- and Y-directions in fixed frame, ρ_f – the constant density of base fluid, P – the pressure, ν – the kinematic viscosity, σ – the electrical conductivity, T – the temperature, C – the concentration, D_B – the Brownian diffusion coefficient, D_T – the thermophoretic diffusion coefficient, and $\tau = (\rho c)_p/(\rho c)_f$ – the ratio of the effective heat capacity of the nanoparticle material and heat capacity of the fluid with ρ being the density, c – the volumetric volume expansion coefficient, and ρ_p – the density of the particles..

Since in the laboratory frame (X, Y), the flow is unsteady, but in a co-ordinate system moving with the wave speed, c, (the wave frame) the motion is steady. The co-ordinates and velocities in two frames are related by the following transformation:

$$x=X-ct,\quad y=Y,\quad u=U-c,\quad v=V,\quad \text{and}\quad p(x,y)=P(X,Y,t) \tag{7}$$

Defining the following transformation:

$$\overline{x}=\frac{x}{\lambda},\ \overline{y}=\frac{y}{d_1},\ \overline{u}=\frac{u}{c},\ \overline{v}=\frac{v}{c\delta},\ \delta=\frac{d_1}{\lambda},\ d=\frac{d_2}{d_1},\ \overline{p}=\frac{d_1^2 p}{\mu c\lambda},\ \overline{t}=\frac{ct}{\lambda},\ h_1=\frac{H_1}{d_1}$$
$$h_2=\frac{H_2}{d_2},\ a=\frac{a_1}{d_1},\ b=\frac{b_1}{d_1},\ \mathrm{Re}=\frac{\rho_f c d_1}{\mu},\ \theta=\frac{T-T_0}{T_1-T_0},\ \mathrm{Pr}=\frac{\nu}{\alpha}$$
$$Nt=\frac{\tau D_T\left(T_1-T_0\right)}{T_0\nu},\ Nb=\frac{\tau D_B\left(C_1-C_0\right)}{\nu},\ \mathrm{Gr}=\frac{\rho g\alpha d_1^2\left(T_1-T_0\right)}{\mu c} \tag{8}$$
$$\mathrm{Br}=\frac{\rho g\alpha d_1^2\left(C_1-C_0\right)}{\mu c},\ \mathrm{Le}=\frac{\nu}{D_B},\ \gamma=\sqrt{\frac{\mu}{\eta}}d_1,\ M=\sqrt{\frac{\sigma}{\mu}}B_0 d_1$$

With the help of eq. (7) and the transformations (8), eqs. (2)-(6) for a couple stress fluid and nanofluid in wave frame (after dropping bars) take the following form

$$\mathrm{Re}\,\delta\left(u\frac{\partial}{\partial x}+v\frac{\partial}{\partial y}\right)u=-\frac{\partial p}{\partial x}+\nabla^2 u-\frac{1}{\gamma^2}\nabla^4 u-M^2(u+1)+\mathrm{Gr}\,\theta+\mathrm{Br}\,\Phi \tag{9}$$

$$\mathrm{Re}\,\delta^3\left(u\frac{\partial}{\partial x}+v\frac{\partial}{\partial y}\right)v=-\frac{\partial p}{\partial y}+\delta^2\nabla^2 v-\frac{\delta^2}{\gamma^2}\nabla^4 v \tag{10}$$

$$\mathrm{Re}\,\delta\left(u\frac{\partial\theta}{\partial x}+v\frac{\partial\theta}{\partial y}\right)=\frac{1}{\mathrm{Pr}}\left(\frac{\partial^2\theta}{\partial y^2}+\delta^2\frac{\partial^2\theta}{\partial x^2}\right)+Nb\left(\delta^2\frac{\partial\theta}{\partial x}\frac{\partial\Phi}{\partial x}+\frac{\partial\theta}{\partial y}\frac{\partial\Phi}{\partial y}\right)+$$
$$+Nt\left[\delta^2\left(\frac{\partial\theta}{\partial x}\right)^2+\left(\frac{\partial\theta}{\partial y}\right)^2\right] \tag{11}$$

$$\mathrm{Re}\,\delta\mathrm{Le}\left(u\frac{\partial\Phi}{\partial x}+v\frac{\partial\Phi}{\partial y}\right)=\left(\frac{\partial^2\Phi}{\partial y^2}+\delta^2\frac{\partial^2\Phi}{\partial x^2}\right)+\delta^2\frac{Nt}{Nb}\frac{\partial^2\theta}{\partial x^2}+\frac{Nt}{Nb}\frac{\partial^2\theta}{\partial y^2} \tag{12}$$

Now applying the long wave length and low Reynolds number approximations the eqs. (9)-(12) reduces in the form:

$$-\frac{\partial p}{\partial x}+\frac{\partial^2 u}{\partial y^2}-\frac{1}{\gamma^2}\frac{\partial^4 u}{\partial y^4}-M^2(u+1)+\mathrm{Gr}\,\theta+\mathrm{Br}\,\Phi=0 \tag{13}$$

$$-\frac{\partial p}{\partial y}=0 \tag{14}$$

$$\frac{1}{\mathrm{Pr}}\frac{\partial^2\theta}{\partial y^2}+Nb\frac{\partial\theta}{\partial y}\frac{\partial\Phi}{\partial y}+Nt\left(\frac{\partial\theta}{\partial y}\right)^2=0 \tag{15}$$

$$\frac{\partial^2\Phi}{\partial y^2}+\frac{Nt}{Nb}\frac{\partial^2\theta}{\partial y^2}=0 \tag{16}$$

The corresponding dimension less boundary conditions which governed the flow are defined:

$$\begin{aligned} &u=-1,\quad v=\frac{\mathrm{d}h_1}{\mathrm{d}x},\quad \frac{\partial^2 u}{\partial y^2}=0\quad \text{at}\quad y=h_1=1+a\cos 2\pi x\\ &u=-1,\quad v=\frac{\mathrm{d}h_2}{\mathrm{d}x},\quad \frac{\partial^2 u}{\partial y^2}=0\quad \text{at}\quad y=h_2=-d-b\cos\left(2\pi x+\phi\right)\end{aligned} \tag{17}$$

$$\theta=0,\quad \Phi=0\quad \text{at}\quad y=h_1 \tag{18}$$

$$\theta=1,\quad \Phi=1\quad \text{at}\quad y=h_2 \tag{19}$$

The dimensionless mean flow, Q, is defined:

$$Q=F+1+d \tag{20}$$

where

$$F=\int_{h_1}^{h_2}u\mathrm{d}y$$

Solution of the problem

In this section we describe a valuable procedure to calculate the analytical solutions for the present system of linear and non-linear differential equations. From eq. (15) we obtain:

$$\Phi(x,y)=-\frac{Nt}{Nb}\theta+f_1(x)y+f_2(x) \tag{21}$$

where $f_1(x)$ and $f_2(x)$ are two unknow functions which can be evaluated using the boundary conditions. Now substitute eq. (21) into (15) we obtain:

$$\frac{\partial^2\theta}{\partial y^2}+\Pr Nbf_1(x)\frac{\partial\theta}{\partial y}=0 \tag{22}$$

The exact solution of eq. (22) give the temperature distribution:

$$\theta(x,y)=\frac{f_3(x)}{\Pr Nbf_1(x)}+f_4(x)\mathrm{e}^{-\Pr Nbf_1(x)y} \tag{23}$$

where $f_3(x)$ and $f_4(x)$ are two unknown functions. Now with the help of temperature distribution, eq. (23), the nano-particle concentration, Φ, is given from eq. (21):

$$\Phi(x,y)=-\frac{Nt}{Nb}\left(\frac{f_3(x)}{\Pr Nbf_1(x)}+f_4(x)\mathrm{e}^{-\Pr Nbf_1(x)y}\right)+f_1(x)y+f_2(x) \tag{24}$$

Now calculate the values of unknown functions $f_1(x), f_2(x), f_3(x)$, and $f_4(x)$ by applying the boundary conditions. In order to calculate the values of $f_1(x)$ and $f_2(x)$ using boundary conditions for θ and Φ on eq. (21) and this gives:

$$f_1(x)=\frac{1+\dfrac{Nt}{Nb}}{h_2-h_1},\qquad f_2(x)=-h_1\left(\frac{1+\dfrac{Nt}{Nb}}{h_2-h_1}\right) \tag{25}$$

For calculating the values of $f_3(x)$ and $f_4(x)$ we apply the boundary conditions for Φ on eq. (24) and this gives:

$$\begin{aligned} f_3(x)&=-\Pr Nbf_1(x)\left(\frac{\mathrm{e}^{-\Pr Nbf_1(x)h_1}}{\mathrm{e}^{-\Pr Nbf_1(x)h_2}-\mathrm{e}^{-\Pr Nbf_1(x)h_1}}\right)\\ f_4(x)&=\frac{1}{\mathrm{e}^{-\Pr Nbf_1(x)h_2}-\mathrm{e}^{-\Pr Nbf_1(x)h_1}}\end{aligned} \tag{26}$$

Thus the exact expressions for the temperature distribution θ and nano-particle concentration Φ are given:

$$\theta(x,y)=\frac{\mathrm{e}^{-\Pr Nbf_1(x)y}-\mathrm{e}^{-\Pr Nbf_1(x)h_1}}{\mathrm{e}^{-\Pr Nbf_1(x)h_2}-\mathrm{e}^{-\Pr Nbf_1(x)h_1}} \tag{27}$$

$$\Phi(x,y)=\left(1+\frac{Nt}{Nb}\right)\left(\frac{y-h_1}{h_2-h_1}\right)-\frac{Nt}{Nb}\left(\frac{\mathrm{e}^{-\Pr Nbf_1(x)y}-\mathrm{e}^{-\Pr Nbf_1(x)h_1}}{\mathrm{e}^{-\Pr Nbf_1(x)h_2}-\mathrm{e}^{-\Pr Nbf_1(x)h_1}}\right) \tag{28}$$

With the help of eqs. (27) and (28) the solution of velocity is obtained from eq. (13) and is defined:

$$\begin{aligned} u=&A\cosh\left(m_1y\right)+A_1\sinh\left(m_1y\right)+A_2\cosh\left(m_2y\right)+A_3\sinh\left(m_2y\right)+\\ &+\frac{a_1\mathrm{Br}\left(y-h_1\right)+a_3-M^2-\dfrac{\mathrm{d}p}{\mathrm{d}x}}{M^2}+\frac{\gamma^2\left(\mathrm{Gr}Nb-\mathrm{Br}Nt\right)\mathrm{e}^{-f_1(x)\Pr yNb}}{a_0Nb\left\{\left[f_1(x)\Pr Nb\right]^4-\left[\gamma f_1(x)\Pr Nb\right]^2+\gamma^2M^2\right\}}\end{aligned} \tag{29}$$

where

$$m_1=\left(\frac{\sqrt{\gamma^2-\sqrt{\gamma^4-4\gamma^2M^2}}}{\sqrt{2}}\right),\quad m_2=\left(\sqrt{\frac{\gamma^2}{2}+\frac{1}{2}\sqrt{\gamma^4-4\gamma^2M^2}}\right) \tag{30}$$

and a_0, a_1, a_2, a_3, A, A_1, A_2, and A_3 are constants. The constants A, A_1, A_2, and A_3 are calculated with the help of boundary conditions defined in eq. (17). The remaining constants a_0, a_1, a_2, a_3 are used to simplify the equations. These constants are defined in *Appendix*.

From eqs. (20) and (29) the expression for pressure gradient is defined:

$$\frac{\mathrm{d}p}{\mathrm{d}x} = a_4\left[a_5 - a_6 - a_7\left(m_1\left\{m_2^3\left[\mathrm{e}^{f_1(x)h_1\,\mathrm{Pr}\,Nb} - \mathrm{e}^{f_1(x)h_2\,\mathrm{Pr}\,Nb}\right] - \left[\mathrm{e}^{f_1(x)h_1\,\mathrm{Pr}\,Nb} + \mathrm{e}^{f_1(x)h_2\,\mathrm{Pr}\,Nb}\right]\cdot\right.\right.$$
$$\cdot\left[f_1(x)\,\mathrm{Pr}\,Nb\right]^3\tanh\left[\frac{1}{2}\left(h_1 - h_2\right)m_2\right]\Big\} + f_1(x)m_2\,\mathrm{Pr}\,Nb\tanh\left[\frac{1}{2}\left(h_1 - h_2\right)m_1\right]\cdot$$
$$\cdot\left[\mathrm{e}^{f_1(x)h_1\,\mathrm{Pr}\,Nb} - \mathrm{e}^{f_1(x)h_2\,\mathrm{Pr}\,Nb}\right]\left\{\left[f_1(x)\,\mathrm{Pr}\,Nb\right]^3 - m_2^2\right\}\coth\left[\frac{1}{2}f_1(x)\left(h_1 - h_2\right)\mathrm{Pr}\,Nb\right] +$$
$$+ m_1^3\left\{-\left[\mathrm{e}^{f_1(x)h_1\,\mathrm{Pr}\,Nb} - \mathrm{e}^{f_1(x)h_2\,\mathrm{Pr}\,Nb}\right]\right\}\left\{m_2 - f_1(x)\,\mathrm{Pr}\,Nb\tanh\left[\frac{1}{2}\left(h_1 - h_2\right)m_2\right]\cdot\right.$$
$$\left.\left.\cdot\coth\left[\frac{1}{2}f_1(x)\left(h_1 - h_2\right)\mathrm{Pr}\,Nb\right]\right\}\right) + F\Bigg] \tag{31}$$

The non-dimensional expression for the pressure rise per wavelength is defined:

$$\Delta p = \int_0^1\left(\frac{\mathrm{d}p}{\mathrm{d}x}\right)\mathrm{d}x \tag{32}$$

where the constants appearing in eqs. (31) and (32) are defined in *Appendix*.

Expressions for different wave shape

The non-dimensional expressions for five considered wave form are given by [18]. The expression for the triangular, square and trapezoidal wave are derived from the Fourier series:

– sinusoidal wave

$$h_1(x) = 1 + a\sin 2\pi x,\quad h_2(x) = -d - b\sin(2\pi x + \phi)$$

– multisinusoidal wave

$$h_1(x) = 1 + a\sin 2n\pi x,\quad h_2(x) = -d - b\sin(2n\pi x + \phi)$$

– triangular wave

$$h_1(x) = 1 + a\left\{\frac{8}{\pi^3}\sum_{m=1}^{\infty}\frac{(-1)^{m+1}}{(2m-1)^2}\sin\left[2\pi(2m-1)x\right]\right\}$$

$$h_2(x) = -d - b\left\{\frac{8}{\pi^3}\sum_{m=1}^{\infty}\frac{(-1)^{m+1}}{(2m-1)^2}\sin\left[2\pi(2m-1)x + \phi\right]\right\}$$

– trapezoidal wave

$$h_1(x) = 1 + a\left\{\frac{32}{\pi^2}\sum_{m=1}^{\infty}\frac{\sin\frac{\pi}{8}(2m-1)}{(2m-1)^2}\sin\left[2\pi(2m-1)x\right]\right\}$$

$$h_2(x) = -d - b\left[\frac{32}{\pi^2}\sum_{m=1}^{\infty}\frac{\sin\frac{\pi}{8}(2m-1)}{(2m-1)^2}\sin\left[2\pi(2m-1)x+\phi\right]\right]$$

– square wave

$$h_1(x) = 1 + a\left[\frac{4}{\pi}\sum_{m=1}^{\infty}\frac{(-1)^{m+1}}{(2m-1)}\cos\left[2(2m-1)\pi x\right]\right]$$

$$h_2(x) = -d - b\left\{\frac{4}{\pi}\sum_{m=1}^{\infty}\frac{(-1)^{m+1}}{(2m-1)}\cos\left[2(2m-1)\pi x+\phi\right]\right\}$$

Numerical results and discussion

The most important intention of this section is to discuss the graphical significances of the current flow problem. In order to calculate the expressions for pressure rise and pressure gradient mathematics software mathematica is used. To see the behavior of pressure rise with volume flow rate figs. 1-6 are plotted by taking different physical parameters of interest.

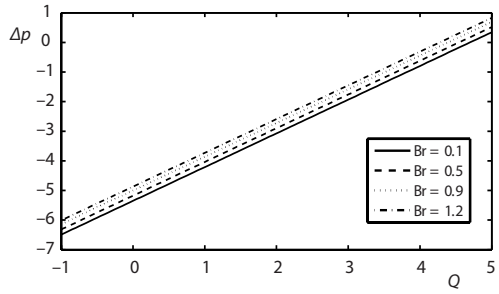

Figure 1. Variation of pressure rise with volume flow rate Q for different values of Br for fixed values of $a = 0.5$, $b = 0.7$, $d = 1.8$, $\phi = \pi/4$, $\gamma = 4.5$, Pr = 0.8, Gr = 0.5, $Nt = 0.5$, $Nb = 0.9$, $M = 0.5$

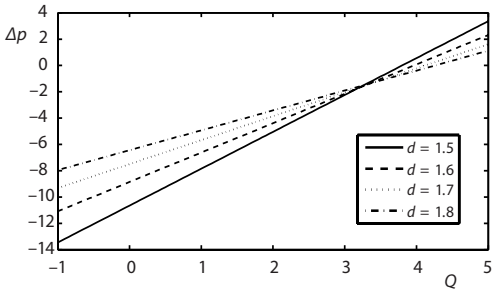

Figure 2. Variation of pressure rise with volume flow rate Q for different values of d for fixed values of $a = 0.7$, $b = 0.7$, Br = 0.9, $\phi = \pi/4$, $\gamma = 3.5$, Pr = 0.5, Gr = 0.8, $Nt = 0.9$, $Nb = 0.5$, $M = 0.5$

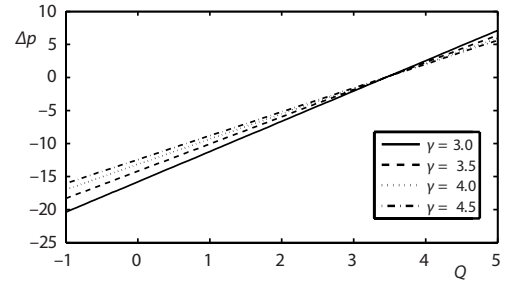

Figure 3. Variation of pressure rise with volume flow rate Q for different values of γ for fixed values of $a = 0.5$, $b = 0.7$, $d = 1.2$, Br = 0.9, $\phi = \pi/4$, Pr = 0.8, Gr = 0.5, $Nt = 0.5$, $Nb = 0.9$, $M = 0.5$

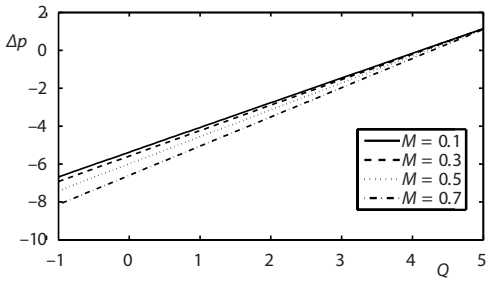

Figure 4. Variation of pressure rise with volume flow rate Q for different values of M for fixed values of $a = 0.5$, $b = 0.7$, $d = 1.7$, Br = 0.9, $\gamma = 3.5$, $\phi = \pi/4$, Pr = 0.5, Gr = 0.8, $Nt = 0.9$, $Nb = 0.5$

Figure 1 shows the variation of pressure rise with volume flow rate Q for different values of Br. It is observed from fig. 1 that the behavior of pressure rise in all the regions, augmented pumping ($\Delta p < 0$, $Q > 0$), retrograde pumping ($\Delta p > 0$, $Q < 0$), and peristaltic pumping ($\Delta p > 0$,

$Q > 0$) are same. Here pressure rise increases with an increase in the values of Br. Figures 2 and 3 shows the behavior of pressure rise for different values of width of channel d and couple stress parameter γ. It is depicted from figs. 2 and 3 that in the peristaltic pumping ($\Delta p > 0$, $Q > 0$) region the pressure rise decreases with an increase in the values of d and γ, while in the augmented pumping ($\Delta p < 0$, $Q > 0$) region the pressure rise increases with an increase in the values of d and γ but there is no variation observed in the retrograde pumping ($\Delta p > 0$, $Q < 0$) region. Figures 4 and 5 are displayed to see the behavior of pressure rise for different values of M and amplitude ratio ϕ.

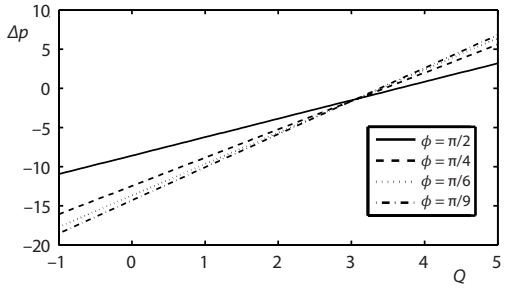

Figure 5. Variation of pressure rise with volume flow rate Q for different values of ϕ for fixed values of $a = 0.5$, $b = 0.7$, $d = 1.2$, Br = 0.8, $\gamma = 4.5$, Pr = 0.5, Gr = 0.5, $Nt = 0.5$, $Nb = 0.9$, $M = 0.5$

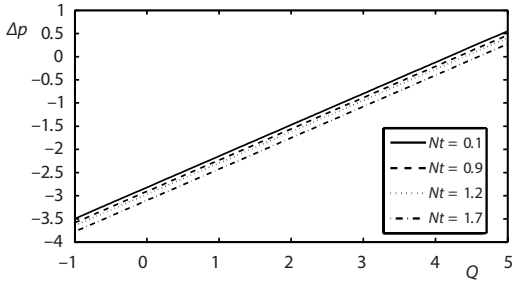

Figure 6. Variation of pressure rise with volume flow rate Q for different values of Nt for fixed values of $a = 0.5$, $b = 0.5$, $d = 2$, $\phi = \pi/6$, Br = 0.9, $\gamma = 4.5$, Pr = 1, Gr = 0.8, $Nb = 0.9$, $M = 0.1$

It is observed from figs. 4 and 5 that in the peristaltic pumping ($\Delta p > 0$, $Q > 0$) region the pressure rise increases with an increase in the values of M and ϕ, while in the augmented pumping ($\Delta p < 0$, $Q > 0$) region the pressure rise decreases with an increase in the values of M and ϕ but there is no variation observed in the retrograde pumping ($\Delta p > 0$, $Q < 0$) region. Figure 6 show the variation of pressure rise for different values of Nt. It is observed from fig. 6 that the behavior of pressure rise in all the regions are same. Here pressure rise decreases with an increase in the values of Nt.

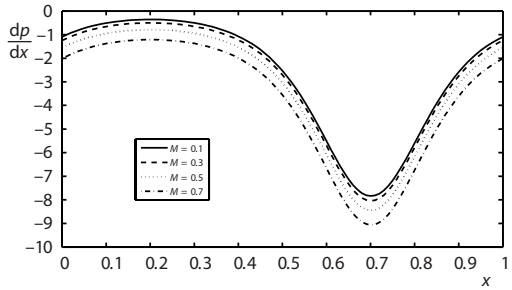

Figure 7. Variation of pressure gradient dp/dx with x for different values of M for fixed values of $a = 0.5$, $b = 0.7$, $d = 2$, $\phi = \pi/6$, Br = 0.7, $\gamma = 4.5$, Pr = 0.5, Gr = 0.8, $Nt = 0.9$, $Nb = 0.5$, $Q = 1$

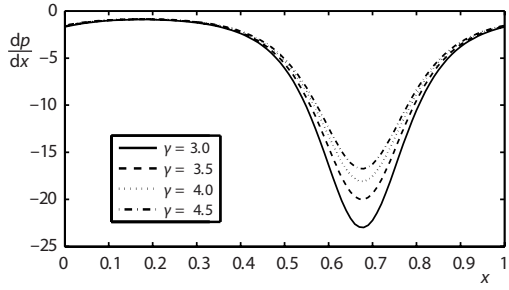

Figure 8. Variation of pressure gradient dp/dx with x for different values of γ for fixed values of $a = 0.5$, $b = 0.7$, $d = 1.2$, $\phi = \pi/4$, Br = 0.9, Pr = 0.8, Gr = 0.5, $Nt = 0.5$, $Nb = 0.9$, $Q = 5$, $M = 0.5$

Figures 7-11 indicate the pressure gradient for different value of M, γ, Br, d, and Q. It is depicted that for $x \in [0, 0.2]$ and $x \in [0.8, 1]$ the pressure gradient is small *i. e*., the flow can easily pass without imposition of a large pressure gradient, while in the region $x \in [0.2, 0.8]$ pressure gradient decreases with an increase in M and increases with an increase in γ, Br, and d, large amount of pressure gradient is required to maintain the flux to pass.

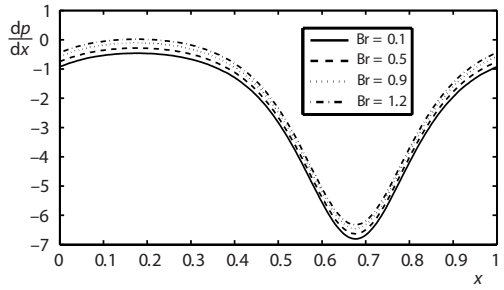

Figure 9. Variation of pressure gradient dp/dx with x for different values of Br for fixed values of a = 0.5, b = 0.7, d = 1.8, $\phi = \pi/4$, Pr = 0.8, Gr = 0.8, Nt = 0.5, Nb = 0.9, Q = 2, M = 0.1, γ = 4.5

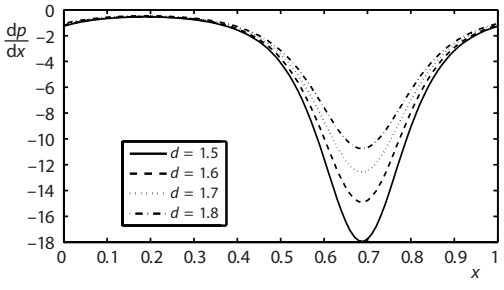

Figure 10. Variation of pressure gradient dp/dx with x for different values of d for fixed values of a = 0.7, b = 0.7, Br = 0.9, $\phi = \pi/4$, Pr = 0.5, Gr = 0.8, Nt = 0.9, Nb = 0.5, Q = 2, M = 0.5, γ = 3.5

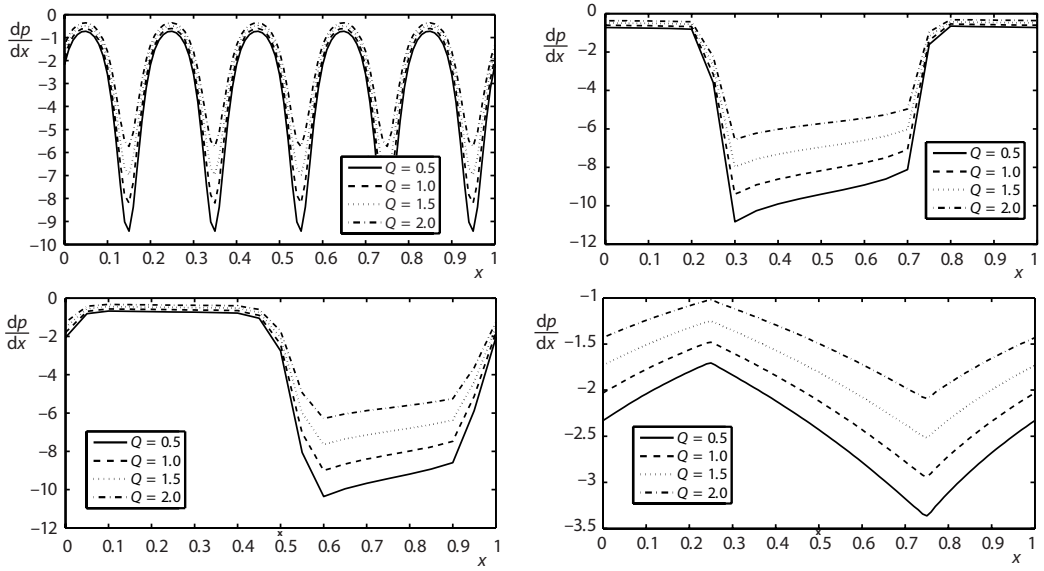

Figure 11. Variation of pressure gradient dp/dx with x for different values wave forms; the other parameters values are a = 0.9, b = 0.1, d = 1.8, Br = 0.9, $\phi = \pi/4$, Pr = 1, Gr = 0.8, Nt = 0.9, Nb = 0.5, M = 0.1, γ = 3.5

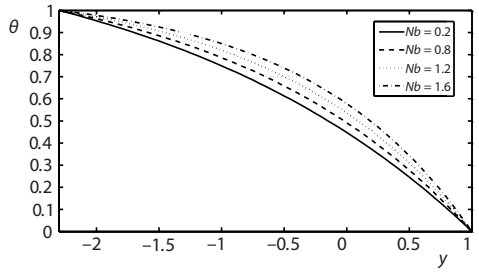

Figure 12. Temperature profile for different values of Nb for fixed values of a = 0.5, b = 1.0, d = 1.8, $\phi = \pi/6$, Pr = 1, Nt = 0.9, x = 0

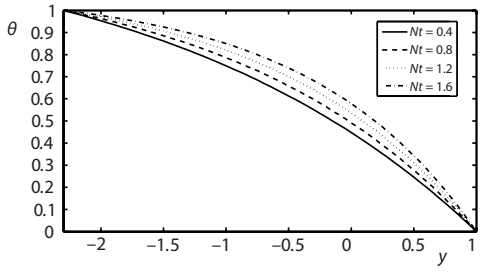

Figure 13. Temperature profile for different values of Nt for fixed values of a = 0.5, b = 1.0, d = 1.8, $\phi = \pi/6$, Pr = 1, Nb = 0.9, x = 0

Figure 11 indicate the pressure gradient for different wave forms. The behavior of temperature profile for different values of *Nb*, *Nt*, and Prandtl number are shown in figs. 12-14. It is observed from figs. 12-14 that temperature profile decreases with an increase in the values of *Nb* and increases with an increase in *Nt* and Prandtl number. This is physically valid because the

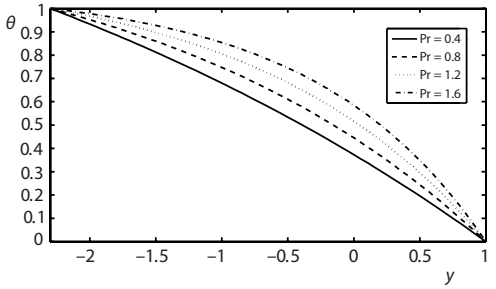

Figure 14. Temperature profile for different values of Pr for fixed values of $a = 0.5$, $b = 1.0$, $d = 1.8$, $\phi = \pi/6$, $Nt = 0.7$, $Nb = 0.9$, $x = 0$

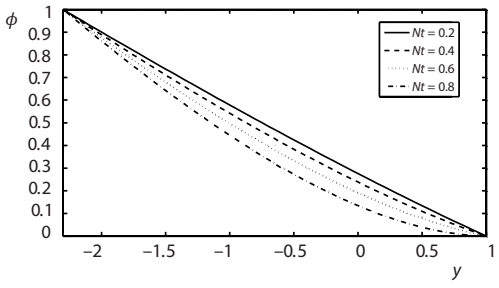

Figure 15. Concentration profile for different values of *Nt* for fixed values of $a = 0.5$, $b = 1.0$, $d = 1.8$, $\phi = \pi/6$, Pr = 1, $Nb = 0.9$, $x = 0$

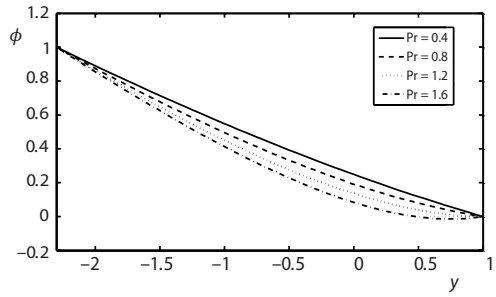

Figure 16. Concentration profile for different values of Pr for fixed values of $a = 0.5$, $b = 1.0$, $d = 1.8$, $\phi = \pi/6$, $Nt = 0.7$, $Nb = 0.9$, $x = 0$

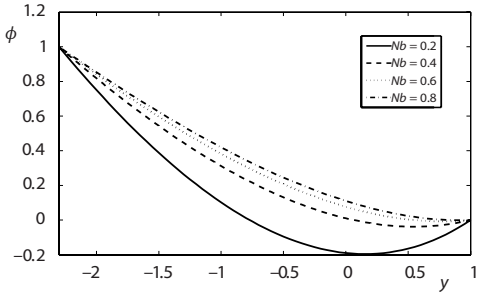

Figure 17. Concentration profile for different values of *Nb* for fixed values of $a = 0.5$, $b = 1.0$, $d = 1.8$, $\phi = \pi/6$, Pr = 0.9, $Nt = 0.9$, $x = 0$

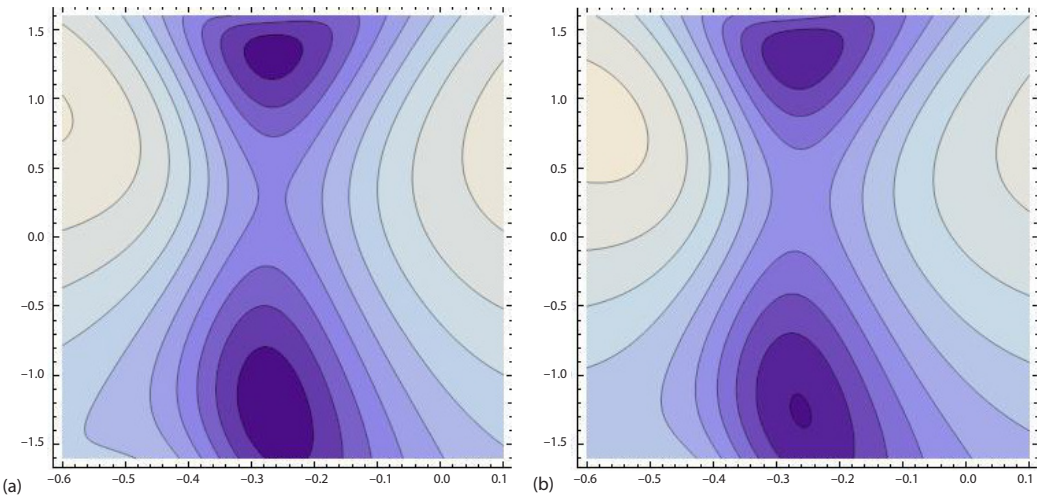

Figure 18. Stream lines for different values of *Nt*; (a) when $Nt = 6$ and (b) when $Nt = 4$; the values of other parameters are $a = 0.5$, $b = 0.7$, $d = 2$, Br = 0.8, $\phi = \pi/4$, Pr = 0.8, Gr = 0.5, $Nb = 0.7$, $M = 1$, $Q = 1.4$, $\gamma = 3$

parameter *Nb* show an inverse relationship and *Nt* and Prandtl number shows direct relationship with temperature. In order to see the effects of concentration profile for different values of *Nb*, *Nt*, and Prandtl number, figs. 15-17 are displayed.

It is depicted from figs. 15-17 that concentration profile show opposite behavior as compared with the temperature profile. In these figures the concentration profile increases with an increase in the values of *Nb* and decreases with an increase in *Nt* and Prandtl number.

Stream lines for different values of *Nt*, γ, and *M* are shown in figs. 18-20. It is depicted from figs. 18 and 19 that the size and number of the trapping bolus increases with the decrease in the values of *Nt* and γ. It is observed form fig. 20 that the size of the trapping bolus increases in the upper half of the channel while in the lower half of the channel the size and number of trapping bolus increases with an increase in *M*. Stream lines for different wave forms are shown in fig. 21.

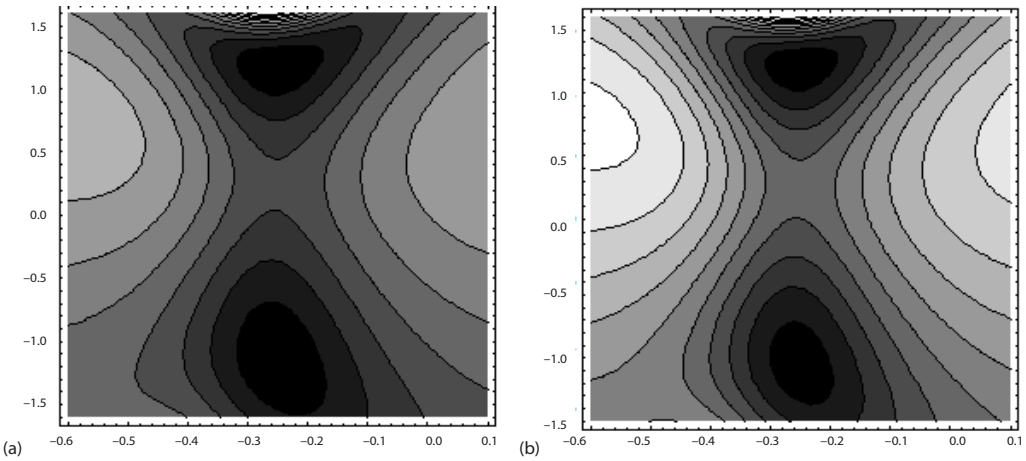

Figure 19. Stream lines for different values of γ; (a) for γ = 4.3 and (b) for γ = 4; the values of other parameters are *a* = 0.5, *b* = 0.7, *d* = 2, Br = 0.8, $\phi = \pi/6$, Pr = 0.8, Gr = 0.5, *Nt* = 0.5, *Nb* = 0.9, *Q* = 2, *M* = 1

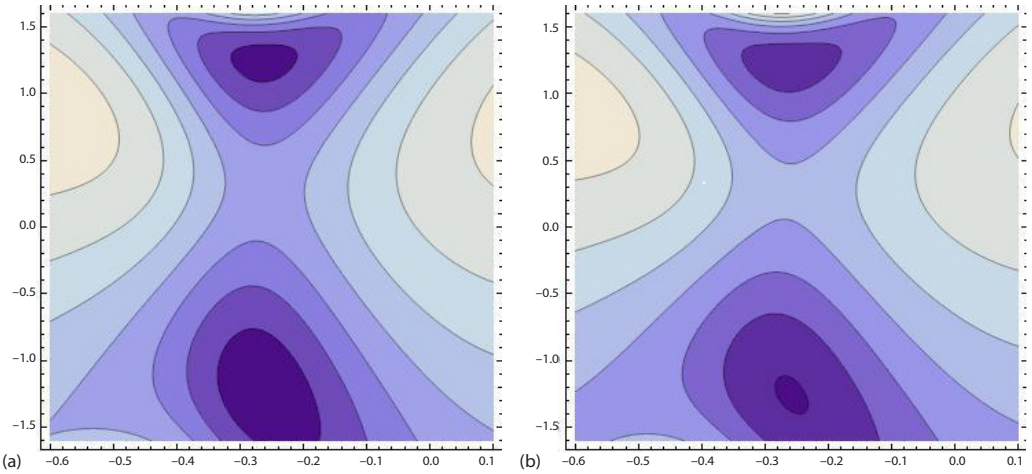

Figure 20. Stream lines for different values of *M*; (a) for *M* = 1.2 and (b) for *M* = 1.4; the values of other parameters are *a* = 0.5, *b* = 0.7, *d* = 2, Br = 0.8, $\phi = \pi/4$, Pr = 0.8, Gr = 0.5, *Nt* = 0.6, *Nb* = 0.7, *Q* = 1.6, γ = 3.5

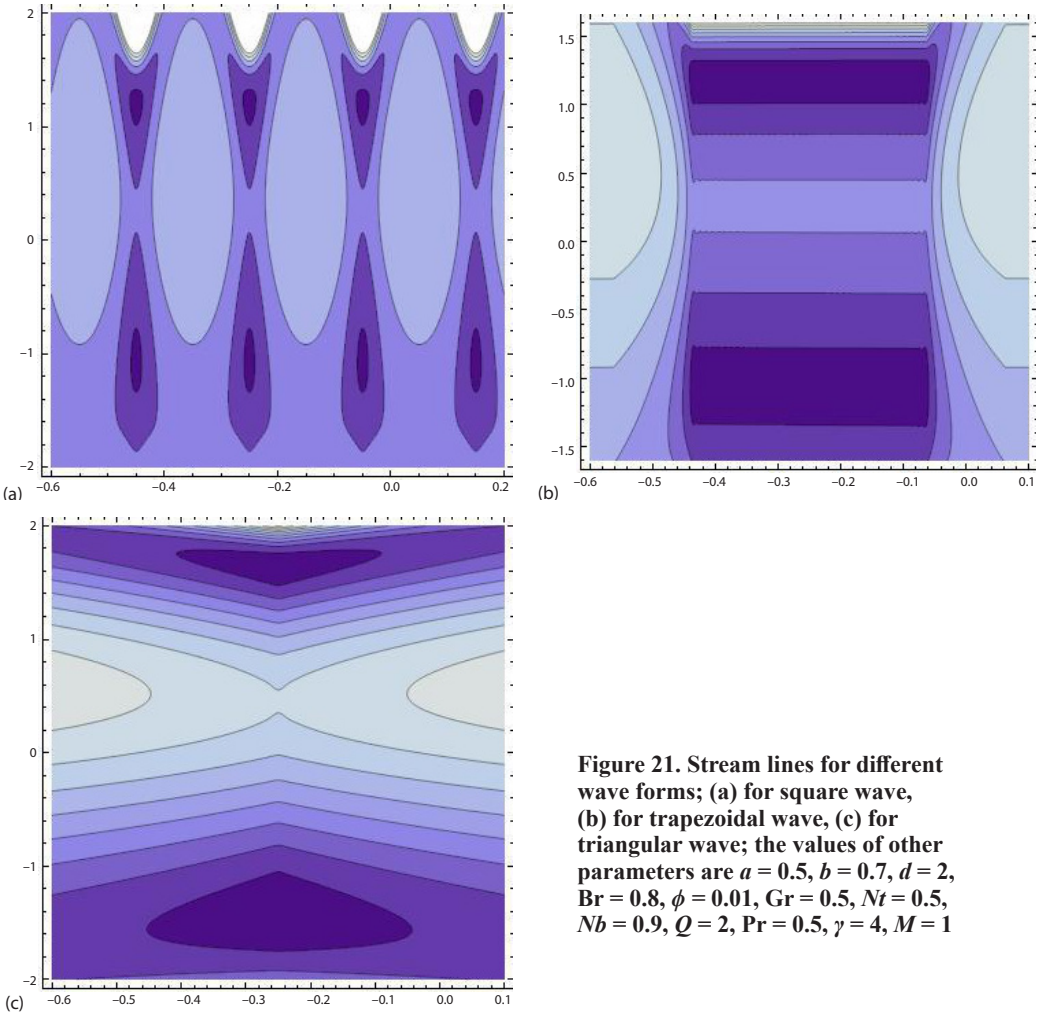

Figure 21. Stream lines for different wave forms; (a) for square wave, (b) for trapezoidal wave, (c) for triangular wave; the values of other parameters are $a = 0.5$, $b = 0.7$, $d = 2$, Br = 0.8, $\phi = 0.01$, Gr = 0.5, $Nt = 0.5$, $Nb = 0.9$, $Q = 2$, Pr = 0.5, $\gamma = 4$, $M = 1$

Conclusions

In this article effects of nanoparticles and magnetic field on peristaltic flow of a couple stress fluid with different wave forms are described. Mathematical modelling of the present flow problem is discussed in detail with nanofluid. Under the assumptions of long wavelength and low Reynolds number approximation we get coupled non-linear differential equations. The exact solutions of temperature distribution, the nanoparticle concentration, velocity, stream function and pressure gradient are computed. The main finding of the problem is summarizes as follows:

- It is observed that the behavior of pressure rise in all the regions (augmented pumping ($\Delta p < 0$, $Q > 0$), retrograde pumping ($\Delta p > 0$, $Q < 0$) and peristaltic pumping ($\Delta p > 0$, $Q > 0$) are same and it increases with an increase in the values of Br.
- It is also observed that in the peristaltic pumping ($\Delta p > 0$, $Q > 0$) region the pressure rise decreases with an increase in the values of width of channel, d, and couple stress parameter, γ, while in the augmented pumping ($\Delta p < 0$, $Q > 0$) region the pressure rise increases with an

increase in the values of d and γ but there is no variation observed in the retrograde pumping ($\Delta p > 0$, $Q < 0$) region.

- It is observed that in the peristaltic pumping ($\Delta p > 0$, $Q > 0$) region the pressure rise increases with an increase in the values of M and ϕ, while in the augmented pumping ($\Delta p < 0$, $Q > 0$) region the pressure rise decreases with an increase in the values of M and ϕ but there is no variation observed in the retrograde pumping ($\Delta p > 0$, $Q < 0$) region.
- It is also observed that temperature profile decreases with an increase in the values of Nb and increases with an increase in Nt and Prandtl number. This is physically valid because the parameter Nb show an inverse relationship and Nt and Prandtl number shows direct relationship with temperature.
- It is found that concentration profile show opposite behavior as compared to the temperature profile. The concentration profile increases with an increase in the values of Nb and decreases with an increase in Nt and Prandtl number.
- It is found that the size and number of the trapping bolus increases with the decrease in the values of Nt and γ.
- It is observed that with an increase in M the size of the trapping bolus increases in the upper half of the channel while in the lower half of the channel the size and number of trapping bolus increases.

Nomenclature

Br – nanoparticle Grashof number
b – amplitude of the wave
C – concentration
Gr – local temperature Grashof number
Le – regular Lewis number
M – magnetic parameter
Nb – Brownian motion parameter
P – pressure
Q – volume flow rate
Re – Reynolds number
T – temperature
U, V – velocities in X- and Y-directions in fixed frame

Greek symbols

γ – couple stress parameter
δ – dimensionless wave number
μ – viscosity
ν – kinematic viscosity
Φ – nanopractic concentration
Ψ – stream function

Appendix

$$a_1 = \frac{1}{h_2 - h_1}\left(1 + \frac{Nt}{Nb}\right), \quad a_2 = \frac{\mathrm{e}^{-f_1(x)h_1 \,\mathrm{Pr}\, Nb}}{a_0}, \quad a_3 = \frac{a_2 \mathrm{Br} Nt}{Nb} - a_2 \mathrm{Gr}$$

$$a_4 = \frac{m_1 m_2 \left(m_1^2 - m_2^2\right) M^2}{\left(h_1 - h_2\right) m_2 \left(m_1^2 - m_2^2\right) m_1 - 2m_1^3 \tanh\left[\frac{1}{2}\left(h_1 - h_2\right) m_2\right] + 2m_2^3 \tanh\left[\frac{1}{2}\left(h_1 - h_2\right) m_1\right]}$$

$$a_5 = -\frac{\left[a_1 \mathrm{Br}\left(h_2 - h_1\right) + 2a_3\right]\left\{m_1^3 \tanh\left[\frac{1}{2}\left(h_1 - h_2\right) m_2\right] - m_2^3 \tanh\left[\frac{1}{2}\left(h_1 - h_2\right) m_1\right]\right\}}{m_1 m_2 \left(m_1^2 - m_2^2\right) M^2}$$

$$a_6 = -\frac{\left(h_1 - h_2\right)\left[a_1 \mathrm{Br}\left(h_1 - h_2\right) - 2a_3 + 2M^2\right]}{2M^2}$$

$$a_7 = \frac{\gamma^2\left(\mathrm{Gr}Nb - \mathrm{Br}Nt\right)}{\left\{\begin{array}{c} f_1(x)m_1m_2\left(m_1^2 - m_2^2\right)\mathrm{Pr}\,Nb^2\left[\mathrm{e}^{-f_1(x)h_1\,\mathrm{Pr}\,Nb} - \mathrm{e}^{-f_1(x)h_2\,\mathrm{Pr}\,Nb}\right] \\ \left(\left[f_1(x)\,\mathrm{Pr}\,Nb\right]^4 - \left[\gamma f_1(x)\,\mathrm{Pr}\,Nb\right]^2 + \gamma^2M^2\right) \end{array}\right\}}$$

$$a_8 = \frac{\mathrm{e}^{-f_1\left[\left(h_1+h_2\right)x\right]\mathrm{Pr}\,Nb}}{a_0\left(m_1^2 - m_2^2\right)M^2Nb\left\{\left(f_1(x)\,\mathrm{Pr}\,Nb\right)^4 - \left[\gamma f_1(x)\,\mathrm{Pr}\,Nb\right]^2 + \gamma^2M^2\right\}}$$

$$a_9 = \frac{\mathrm{csch}\left[\left(h_1 - h_2\right)m_1\right]}{m_2^2 - m_1^2}$$

$$a_{10} = \left[\cosh\left(h_2m_1\right)\mathrm{e}^{f_1(x)h_2\,\mathrm{Pr}\,Nb} - \cosh\left(h_1m_1\right)\mathrm{e}^{f_1(x)h_1\,\mathrm{Pr}\,Nb}\right]$$

$$a_{11} = \frac{\mathrm{csch}\left[\left(h_1 - h_2\right)m_2\right]}{m_1^2 - m_2^2}$$

$$a_{12} = \left[\cosh\left(h_2m_2\right)\mathrm{e}^{f_1(x)h_2\,\mathrm{Pr}\,Nb} - \cosh\left(h_1m_2\right)\mathrm{e}^{f_1(x)h_1\,\mathrm{Pr}\,Nb}\right]$$

$$A = a_8\mathrm{csch}\left[\left(h_1 - h_2\right)m_1\right]\left(\gamma^2M^2\left(\mathrm{Gr}Nb - \mathrm{Br}Nt\right)\left[\sinh\left(h_1m_1\right)e^{f_1(x)h_1\,\mathrm{Pr}\,Nb} - \sinh\left(h_2m_1\right)e^{f_1(x)h_2\,\mathrm{Pr}\,Nb}\right]\cdot\right.$$
$$\left.\cdot\left[m_2^2 - \left(f_1(x)\,\mathrm{Pr}\,Nb\right)^2\right] - a_0m_2^2Nbe^{f_1\left[\left(h_1+h_2\right)x\right]\mathrm{Pr}\,Nb}\left\{\sinh\left(h_1m_1\right)\left[a_1\mathrm{Br}\left(h_1 - h_2\right) - a_3 + \frac{\mathrm{d}p}{\mathrm{d}x}\right] + \right.\right.$$
$$\left.\left. + \left(a_3 - \frac{\mathrm{d}p}{\mathrm{d}x}\right)\sinh\left(h_2m_1\right)\right\}\left\{\left[f_1(x)\,\mathrm{Pr}\,Nb\right]^4 - \left[\gamma f_1(x)\,\mathrm{Pr}\,Nb\right]^2 + \gamma^2M^2\right\}\right)$$

$$A_1 = a_9\left(\frac{\gamma^2\left(\mathrm{Gr}Nb - \mathrm{Br}Nt\right)\mathrm{e}^{-f_1\left[\left(h_1+h_2\right)x\right]\mathrm{Pr}\,Nb}\left\{\left[f_1(x)\,\mathrm{Pr}\,Nb\right]^2 - m_2^2\right\}a_{10}}{a_0Nb\left\{\left[f_1(x)\,\mathrm{Pr}\,Nb\right]^4 - \left[\gamma f_1(x)\,\mathrm{Pr}\,Nb\right]^2 + \gamma^2M^2\right\}} + \right.$$
$$\left. + \frac{m_2^2\left\{\cosh\left(h_1m_1\right)\left[a_1\mathrm{Br}\left(h_2 - h_1\right) + a_3 - \frac{\mathrm{d}p}{\mathrm{d}x}\right] + \left(\frac{\mathrm{d}p}{\mathrm{d}x} - a_3\right)\cosh\left(h_2m_1\right)\right\}}{M^2}\right)$$

$$A_2 = a_8\mathrm{csch}\left[\left(h_1 - h_2\right)m_2\right]\left(a_0m_1^2Nbe^{f_1\left[\left(h_1+h_2\right)x\right]\mathrm{Pr}\,Nb}\left\{\sinh\left(h_1m_2\right)\left[a_1\mathrm{Br}\left(h_1 - h_2\right) - a_3 + \frac{\mathrm{d}p}{\mathrm{d}x}\right] + \right.\right.$$
$$\left.\left. + \left(a_3 - \frac{\mathrm{d}p}{\mathrm{d}x}\right)\sinh\left(h_2m_2\right)\right]\left\{\left[f_1(x)\,\mathrm{Pr}\,Nb\right]^4 - \left[\gamma f_1(x)\,\mathrm{Pr}\,Nb\right]^2 + \gamma^2M^2\right\} + \gamma^2M^2\left(\mathrm{Gr}Nb - \mathrm{Br}Nt\right)\cdot\right.$$
$$\left.\cdot\left\{\left[f_1(x)\,\mathrm{Pr}\,Nb\right]^2 - m_1^2\right\}\left[\sinh\left(h_1m_2\right)\mathrm{e}^{f_1(x)h_1\,\mathrm{Pr}\,Nb} - \sinh\left(h_2m_2\right)\mathrm{e}^{f_1(x)h_2\,\mathrm{Pr}\,Nb}\right]\right)$$

$$A_3 = a_{11}\left(\frac{\gamma^2\left(\mathrm{Gr}Nb-\mathrm{Br}Nt\right)\mathrm{e}^{-f_1\left[\left(h_1+h_2\right)x\right]\mathrm{Pr}\,Nb}\left\{\left[f_1(x)\,\mathrm{Pr}\,Nb\right]^2-m_1^2\right\}a_{12}}{a_0Nb\left\{\left[f_1(x)\,\mathrm{Pr}\,Nb\right]^4-\left[\gamma f_1(x)\,\mathrm{Pr}\,Nb\right]^2+\gamma^2M^2\right\}}+\right.$$
$$\left.+\frac{m_1^2\left\{\cosh\left(h_1m_2\right)\left[a_1\mathrm{Br}\left(h_2-h_1\right)+a_3-\dfrac{\mathrm{d}p}{\mathrm{d}x}\right]+\left(\dfrac{\mathrm{d}p}{\mathrm{d}x}-a_3\right)\cosh\left(h_2m_2\right)\right\}}{M^2}\right)$$

References

[1] Choi, S. U. S., Enhancing Thermal Conductivity of Fluid with Nanoparticles Developments and Applications of Non-Newtonian Flow, *ASME FED*, *231* (1995), 66, pp. 99-105
[2] Aziz, A., *et al.*, Free Convection Boundary Layer Flow Past a Horizontal Flat Plate Embedded in Porous Medium Filled by Nanofluid Containing Gyrotactic Microorganisms, *International Journal of Thermal Sciences*, *56* (2012), 48, pp. 48-57
[3] Zeeshan, A., *et al*., Biologically Inspired Transport of Solid Spherical Nanoparticles in an Electrically-Conducting Viscoelastic Fluid with Heat Transfer, *Thermal Science*, *23* (2018), 5, p. 324
[4] Aziz, A., Khan, W. A., Natural Convective Boundary Layer Flow of a Nanofluid Past a Convectively Heated Vertical Plate, *International Journal of Thermal Sciences*, *52* (2012), Feb., pp. 83-90
[5] Waqas, H., *et al*., Analysis on the Bioconvection Flow of Modified Second-Grade Nanofluid Containing Gyrotactic Microorganisms and Nanoparticles, *Journal of Molecular Liquids*, *291* (2019), Oct., 111231
[6] Akram, S., Nadeem, S., Consequence of Nanofluid on Peristaltic Transport of a Hyperbolic Tangent Fluid Model in the Occurrence of Apt (Tending) Magnetic Field, *Journal of Magnetism and Magnetic Materials*, *358-359* (2014), May, pp. 183-191
[7] Akram, S., Nadeem, S., Significance of Nanofluid and Partial Slip on the Peristaltic Transport of a Jeffrey Fluid Model in an Asymmetric Channel with Different Wave Forms, *IEEE Transactions on* Nanotechnology, *13* (2014), 2, pp. 375-385
[8] Akram, S., Effects of Nanofluid on Peristaltic Flow of a Carreau Fluid Model in an Inclined Magnetic Field, *Heat Transfer Asian Research*, *43* (2014), 4, pp. 368-383
[9] Ellahi, R., *et al*., Peristaltic Blood Flow of Couple Stress Fluid Suspended with Nanoparticles under the Influence of Chemical Reaction and Activation Energy, *Symmetry*, *11* (2019), 2, 276
[10] Akbar, N. S., Nadeem, S., Endoscopic Effects on Peristaltic Flow of a Nanofluid, *Communication in Theortical Physics*, *56* (2011), 4, pp. 761-768
[11] Latham, T. W., Fluid Motion in a Peristaltic Pump, M. Sc. thesis, MIT, Cambridge, Mass., USA, 1966
[12] Rashidi, M. M., *et al*., Heat and Mass Transfer Analysis on MHD Blood Flow of Casson Fluid Model Due to Peristaltic Wave, *Thermal Science*, *22* (2018), 6A, pp. 2439-2448
[13] Riaz , A., *et al.*, Effects of External Magnetic Field on Non-Newtonian Two Phase Fluid in an Annulus with Peristaltic Pumping, *Journal of Magnetics*, *24* (2019), 1, pp. 62-69
[14] Bhatti, M. M., *et al*., Effects of Coagulation on the Two-Phase Peristaltic Pumping of Magnetized Prandtl Biofluid through an Endoscopic Annular Geometry Containing a Porous Medium, *Chinese Journal of Physics*, *58* (2010), Apr., pp. 222-234
[15] Ellahi, R., *et al*., A Mathematical Study of Non-Newtonian Micropolar Fluid in Arterial Blood Flow through Composite Stenosis, *Journal of Applied Mathematics and Information Sciences*, *8* (2014), 4, pp. 1567-1573
[16] Ellahi, R., *et al*., Series Solutions of Magnetohydrodynamic Peristaltic Flow of a Jeffrey Fluid in Eccentric Cylinders, *Journal of Applied Mathematics and Information Sciences*, *7* (2013), 4, pp. 1441-1449
[17] Eytan, O., *et al*., Peristaltic Flow in a Tapered Channel: Application to Embryo Transport Within the Uterine Cavity, *Medical Engineering Physics*, *23* (2001), 7, pp. 473-482
[18] Akram, S., *et al*., Effects of Heat and Mass Transfer on Peristaltic Flow of a Bingham Fluid in the Presence of Inclined Magnetic Field and Channel with Different Wave Forms, *Journal of Magnetism and Magnetic Materials*, *362* (2014), Aug., pp. 184-192
[19] Akram, S., Effects of Slip and Heat Transfer on a Peristaltic Flow of a Carreau Fluid in a Vertical Asymmetric Channel, *Computational Mathematics and Mathematical Physics*, *54* (2014), Dec., pp. 1886-1190

[20] Nadeem, S., *et al*., Simulation of Heat and Chemical Reactions on Peristaltic Flow of a Williamson Fluid in an Inclined Asymmetric Channel, *Iranian Journal of Chemistry and Chemical Engineering*, *32* (2013), 2, pp. 93-107
[21] Nadeem, S., Akram, S., Heat Transfer in a Peristaltic Flow of MHD Fluid with Partial Slip, *Communications in Non-Linear Science and Numerical Simulation*, *15* (2010), 2, pp. 312-321
[22] Akram, S., *et al*., Numerical and Analytical Treatment on Peristaltic Flow of Williamson Fluid in the Occurrence of Induced Magnetic Field, *Journal of Magnetism and Magnetic Materials*, *346* (2013), Nov., pp. 142-151
[23] Yldrm, A., Sezer, S. A., Effects of Partial Slip on the Peristaltic Flow of a MHD Newtonian Fluid in an Asymmetric Channel, *Mathematical and Computer Modeling*, *52* (2010), 3-4, pp. 618-625
[24] Haroun, M. H. Non-Linear Peristaltic Flow of a Fourth Grade Fluid in an Inclined Asymmetric Channel, *Computer Material Science*, *39* (2007), 2, pp. 324-333
[25] Haroun, M. H., Effect of Deborah Number and Phase Difference on Peristaltic Transport of a Third Order Fluid in an Asymmetric Channel, *Communications in Non-Linear Science and Numerical Simulation*, *12* (2007), 8, pp. 1464-1480
[26] Srinivas, S., Mixed Convective Heat and Mass Transfer in an Asymmetric Channel with Peristalsis, *Communications in Nonlinear Science and Numerical Simulation*, *16* (2011), 4, pp. 1845-1862
[27] Kothandapani, M., Srinivas, S., Non-Linear Peristaltic Transport of a Newtonian Fluid in an Inclined Asymmetric Channel through a Porous Medium, *Physics Letters A*, *372* (2008), 8, pp. 1265-1276
[28] Nadeem, S., Akram, S., Magnetohydrodynamic Peristaltic Flow of a Hyperbolic Tangent Fluid in a Vertical Asymmetric Channel with Heat Transfer, *Acta Mechanica and Sinica*, *27* (2011), Mar., pp. 237-250
[29] Kothandapani, M., Srinivas, S., Peristaltic Transport of a Jeffrey Fluid under the Effect of Magnetic Field in an Asymmetric Channel, *International Journal of Non-Linear Mechanics*, *43* (2008), 9, pp. 915-924
[30] Riaz, A., *et al*., Mass Transport with Asymmetric Peristaltic Propulsion Coated with Synovial Fluid, *Coatings*, 8 (2018), 11, 407

Paper submitted: July 20, 2019
Paper revised: August 17, 2019
Paper accepted: September 5, 2019